Electrolyte Jet Machining for Surface Texturing of Inconel 718

Mitchell-Smith, J. (a); Murray, J. W. (a); Kunieda, M. (b); Clare, A. T. (a)

(a) -Institute for Advanced Manufacturing, University of Nottingham, Nottingham, United Kingdom

(b) -Department of Engineering, University of Tokyo, Japan

Abstract

Electrolyte jet machining is an emerging non-conventional machining process which is capable of selectively applying multi-scale surface textures. Surfaces processed in this way do not suffer from thermal damage and hence this technique is highly suited to finishing procedures in high value manufacturing across the aerospace and biomedical sectors. Furthermore, input variables can be modified dynamically to create functional graduation across component surfaces.

In this study, the development and design of a custom-built EJM system is described, and the capability of the EJM platform to machine and create surface textures in Inconel 718, a widely used nickel based super alloy, is investigated. Through control of machine path programming and parameter variation, multi-scale surface textures are created which have the potential to enhance bonding with subsequent coating layers and also provide fluid dynamic advantage.

1 Introduction

Electrolyte Jet machining (EJM) is a localised form of Electro Chemical Machining (ECM). In this regard EJM shares the advantages of ECM, whereby materials resistant to sheer based machining methods can be processed easily. EJM is capable of selectively machining material, without the use of masking technology, analogous to laser or waterjet machining. At a sufficient flow rates, a fluidic phenomenon known as ‘hydraulic jump’ occurs at locations distant from the jetted column of fluid directly beneath the nozzle. In EJM, this phenomenon is exploited, and only a thin layer of fluid is present in regions outside of the intended machining area, thereby resulting in a concentrated current density profile immediately beneath the nozzle. The current profile is therefore a concentrated Gaussian distribution [1], which peaks at the centre of the jet. It is this principle which allows precise machining. This is represented in the schematic in Figure 1.

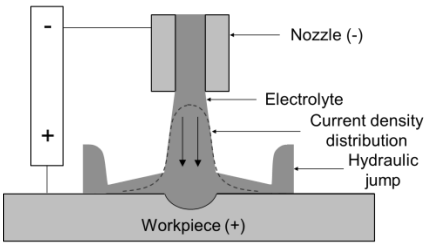

Figure 1: *Schematic of the EJM process*

Thermal and mechanical properties have no influence on machinability by EJM. No residual stress is induced in the material during machining. In addition EJM is able to create net Nano-scale surface structures utilising scalable and relatively low cost technology for high value industries [2]. Although Material Removal Rates (MRR) are currently too small for full part machining, when integrated into process chains EJM is an effective manufacturing tool. Previous work by Kunieda et al. [3] and Hackert-Oschatzchen et al [4] have demonstrated the capability of the process and defined process windows for subtractive machining to achieve defined material removal through simulation and experimental procedure. In this paper a machine utilising the EJM process is demonstrated for the purpose of surface texturing aerospace components. This is desirable as turbine manufacturers seek to produce components which remain clean in service and display enhanced aerodynamic properties. Baseline resolution and repeatability are assessed here for the purpose of creating multi-scale surface textures [5]. To elucidate this, Inconel 718, a nickel based superalloy, commonly used in the aerospace industry is processed in this study. The machining characteristics of Inconel 718 by EJM alongside the capability to surface texture are explored here.

2 Experimental

2.1 Materials and apparatus

The material chosen for demonstration is Inconel 718, composition in Table 1. It is a precipitate strengthened Nickel Chromium based alloy widely used in the gas turbine industry for applications requiring high strength at high temperature with excellent corrosion resistance. These attributes, however, make it difficult to machine by traditional methods.

Table 1: *Inconel 718 composition weight %. (Conforming to AMS specification)*

Ni	*Cr*	*Fe*	*Nb+Ta*	*Mo*	*Ti*	*Al*	*Co*	*C*	*Mn*	*Si+P+S+Cu+B*
52.5	*19*	*17*	*5.125*	*3.05*	*0.9*	*0.6*	*1*	*0.08*	*0.35*	*<1*

Three Parker high precision linear actuators are used to create tool paths in x, y and z axis, with a Diener Precision Gear Pump (Silencer Series) providing the electrolyte flow for the EJM system used here. Both the tool path and electrolyte flow are CNC integrated utilising a Trio Motion Industrial motion controller with tool path generation in Trio Basic, allowing direct importation of CAD data utilising Trio CAD2Motion software for tool path generation achieving end to end facilities for CAD to CAM. Labview is used as the main operator GUI and master control system allowing program selection and parameter control of electrolyte supply, current levels and safety measures from a common interface.

The electrolyte used was a 20%/wt. solution of Sodium Nitrate held in a supply tank and supplied directly to the machine nozzle via the micro-pump. The nozzle is designed to be a consumable part utilising ISO standardised bio medical Luer fitments. Waste solution carrying the debris is captured and stored for disposal. Scanning electron microscopy (SEM) was performed using a Hitachi S-2600N. Profilometry was performed with a Bruker white-light interferometer.

Table 2: *Parameter range used for machining trials*

Current Range (mA)	*Stand-off (µm)*	*Internal Nozzle Diameter (µm)*	*Scan Speed (mm/s)*	*Electrolyte Flow Rate (ml/s)*	*Current density (A/cm2)*	*Electrolyte*
90	*50-250*	*152*	*0.01-100*	*0.54*	*992*	*NaNO3aq 20%wt*

Two parameters were varied in this study; traverse speed and nozzle stand-off (distance between nozzle tip and work-piece surface) in order to produce repeatable surface textures. Scan speeds ranged from 10 microns per second to 100mm per second. Stand-off distance was varied from 50-250 µm in order to assess the compressed air constriction nozzle. The parameters in Table 2 were used in the experiments performed in this work.

3 Results and discussion

3.1 Machining performance with traverse speed and stand-off distance

From initial machining trials, shallow machining with a depth of between 5 and 10 µm was performed. In order to assess the capability to machine deeper cuts, the parameters of traverse speed and stand-off distance were varied and the depths and kerf widths of the resulting cuts were measured. In order to demonstrate the range of traverse speeds possible according to the equipment, a range of speeds were tested, from 0.01 mm/s to 100 mm/s, and the depth and width of the resulting cuts were measured (Figure 2). As expected, depth was observed to decrease with increasing traverse speed. The deepest average cut of 311 µm was produced using the lowest machining speed of 0.01 mm/s, while at a speed of 100 mm/s, an average cut depth of 0.79 µm was machined. As speed decreased from 100 to 1 mm/s, the depth increased close to inversely proportionally; from 0.79 µm at 100 mm/s to 8.4 µm at 10 mm/s, and 64.0 at 1 mm/s.

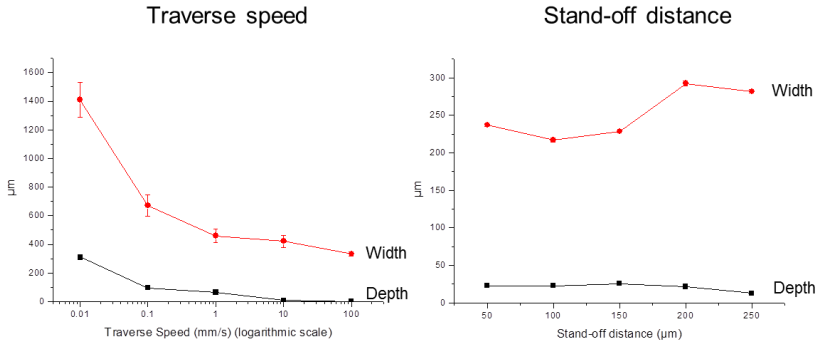

Figure 2: *Variation of depth of cut and kerf-width with changing traverse speed. Errors bars are the standard deviation of the values used to calculate the mean.*

This trend is consistent with a tenfold increase in time the workpiece is subject to the machining jet. With even slower speeds however, the trend was not maintained, although deeper machining still occurred, with 0.1 mm/s yielding a cut depth of 95 µm. This deviation from the trend may be caused by distance between the nozzle and the workpiece effectively increasing during machining, due to material removal. This effect may have caused disruption to the expected jet shape due to the complicated morphology at the surface, thereby changing the current density

profile. SEM images in Figure 3 show the curvature, surface morphology and micro texture of the machined cuts processed between 0.1 and 10 mm/s traverse speed.

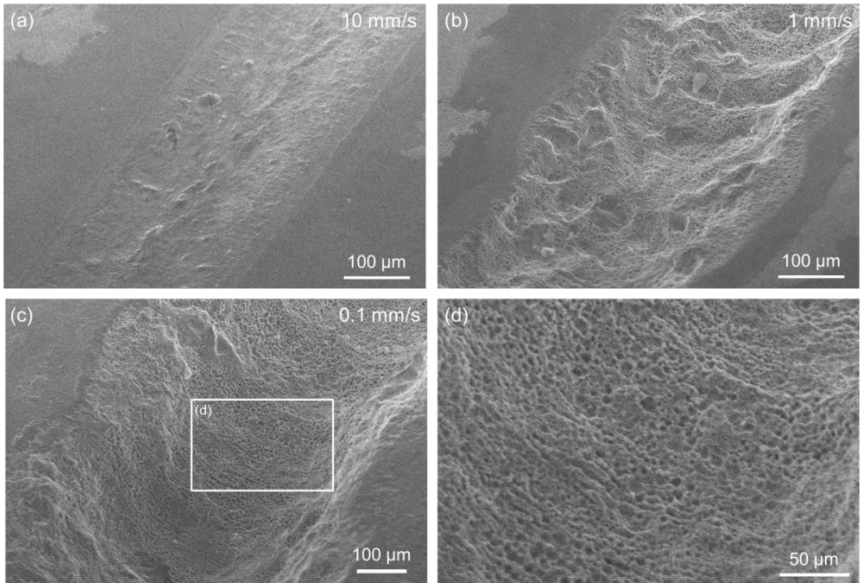

Figure 3: *SEM micrographs images showing kerf produced at varying traverse speed. (d) Shows a detail of resulting micro-surface texture*

As expected the kerf width showed a strong dependence on traverse speed. For example, the fastest speed of 100 mm/s yielded an average kerf width of 333 µm, whereas the slowest speed of 0.01 produced a much higher width of 1410 µm. Between 10 and 1 mm/s speed, however, the widths yielded were relatively similar, at 422 and 460 µm respectively. Interestingly, the mean machined width of 333 µm created by the fastest traverse speed is a ratio of 2.19 of width:nozzle diameter. This matches the ratio of width:nozzle diameter of 2.2 single dimples produced by Hackert-Oschätzen in stainless steel. However with slower speeds, the ratio deviated significantly from this 2.2 value.

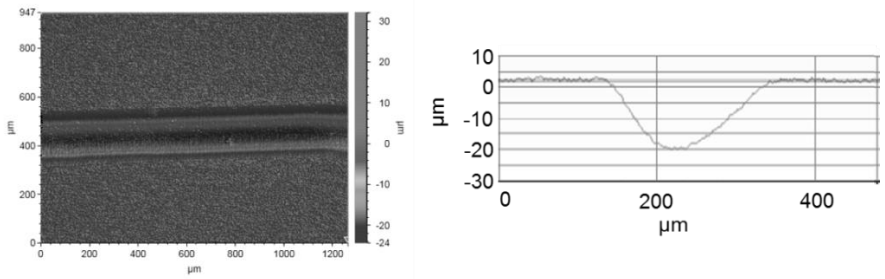

Figure 4: *White-light interferometry surface image and profile of cut using 100 µm stand-off distance*

The effect of stand-off distance on the depth and width of cuts was then evaluated using a traverse speed of 0.5 mm/s. The results are shown in Figure 2. In theory, with a consistent jet shape, the current density reaching the machining area on the workpiece should not vary with stand-off distance. In terms of machined depth, the deepest cut of 25.6 µm was produced using the middle stand-off distance of 150 µm. 100 and 50 µm produced 22.7 and 22.9 µm depth respectively. Therefore based on these results, a stand-off distance roughly equivalent to the internal nozzle diameter, yielded the most efficient machining regime. With the higher stand-offs of 250 and 200 µm, the kerf width was at its highest of 282 and 292 µm respectively, significantly larger than the 229 µm and 237 µm width produced by 150 and 50 µm stand-off respectively. The profile produced using a 100 µm stand-off value is shown in Figure 4. The Gaussian distribution expected by the current density curve is represented clearly by the machined depth profile. If we consider the jet to remain constricted to a column shape directly beneath the nozzle, a change in depth and width with changing stand-off would not be expected. However, jet spread may be occurring, thereby reducing the peak current density in the profile. In further work the effect of jet pressure on jet width should be assessed, to determine the correct flow rate in order to yield a jet which is unaffected by changing stand-off distance.

3.2 Multi-scale surface textures

In Figure 3d), a typical pitted surface texture can be observed on a machined surface, using a slow traverse speed of 0.1 mm/s. Interestingly, this can be discussed in the context of the work by Kawanaka et al. [6] In their work in stainless steel, a more pitted surface was produced when using a lower current density. The pitted surface however in this paper may be explained by the reduced flow of the electrolyte inside the deeper groove, resulting in a longer residency of electrolyte

within the trench.. However, this dynamically changing current density is critical to the introduction of surface textures by EJM and should be investigated further.

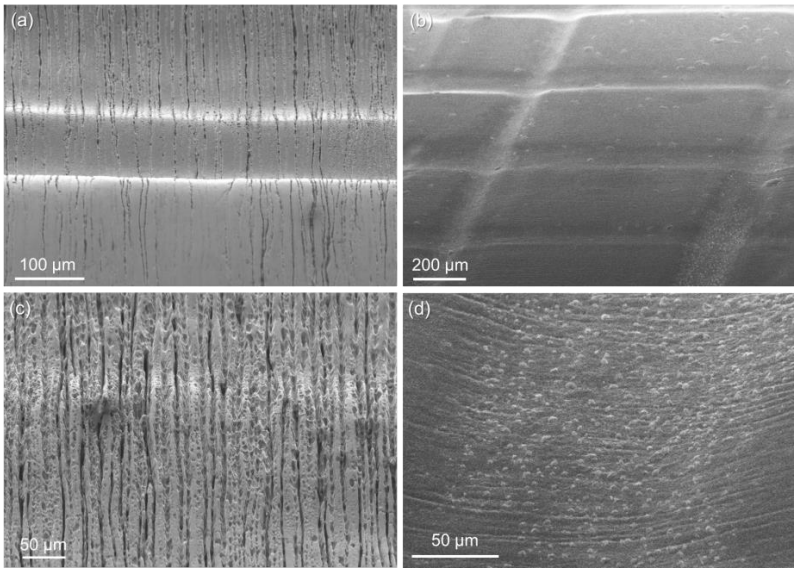

Figure 5: *Sharp groove and hatched pattern produced using EJM. A range of micro textures compliment the form by varying number of passes (c) striations (d) pores*

In Figure 5, grooved and hatched-groove patterns in Inconel 718 are shown. In (c) and (d), high magnification images of the surface textures produced on the bottoms on the grooves of (a) and (b) respectively, can be seen. The groove in figure (a) was produced using 4 repeated machining runs over the same area using a nozzle diameter of 152 µm, whereas the structures in (b) were produced using single runs of the jet with a 250 µm nozzle, both with a stand-off and speed of 100 µm and 0.5 mm/s respectively. Using the larger nozzle the current density is expected to be 2.7 times small than that using the smaller one. In (c) a striated morphology is shown, with striations perpendicular to the direction of jet movement. In the hatched pattern an undulating surface texture was produced. These textures are unique from the pitted surface seen at the bottom of the deep machined groove seen in Figure 3 (d). These results show that with control of machine path programming, surface textures can be varied easily.

4 Conclusions

A new EJM platform has been demonstrated in this study. The process window has been defined for key process input variables of traverse speed and stand-off distance to assess their effect on kerf width and depth of cut for Inconel 718. This was undertaken at constant current density although future developments of the machine tool described here will have the facility to dynamically adjust this. The key findings of this work are detailed below.

- At low traverse speeds (0.1 mm/s) and optimum standoff distance it is possible to record MRRs of $0.5x10^{-12}$ m^3/s. Although greater MRRs can be achieved with lower speeds ensuing a much greater depth of cut the quality and definition of the created feature becomes unacceptable.
- Depth of cut scales inversely linearly with respect to traverse speed, but at 0.1 mm/s and slower, machining becomes less efficient, likely due to changes in electrolyte flow in the machining area as the trench deepens. Stand-off distance also affected depth and width of cut, which is likely due to constriction jet flow variation as this varies.
- EJM of Inconel 718 reveals the creation of a textured surface in addition to the machined profile which varies as a function of number of machining runs and nozzle size, and therefore current density. This is subject to further development to identify process conditions which will allow the generation of graduated surface textures.

Literature

1. Natsu, W., T. Ikeda, and M. Kunieda, *Generating complicated surface with electrolyte jet machining.* Precision Engineering, 2007. **31**(1): p. 33-39.
2. Kawanaka, T., et al., *Selective surface texturing using electrolyte jet machining*, in *2nd CIRP Conference on Surface Integrity (CSI)*. 2014, Elsevier: Nottingham, United Kingdom.
3. Natsu, W., S. Ooshiro, and M. Kunieda, *Research on generation of three-dimensional surface with micro-electrolyte jet machining.* CIRP Journal of Manufacturing Science and Technology, 2008. **1**(1): p. 27-34.
4. Hackert-Oschätzchen, M., et al., *Micro machining with continuous electrolytic free jet.* Precision Engineering, 2012. **36**(4): p. 612-619.
5. Gandhi, R., et al., *Novel methods for scalable manufacturing of micro-textured surfaces*, in *ISERC conference; IIE Annual Conference*. 2014: Montreal, Canada.
6. Kawanaka, T., et al., *Micro Textured Surfaces Created By Electrolyte Jet Machining*, in *5th International Conference of Asian Society for Precision Engineering and Nanotechnology (ASPEN2013)*. 2013: Taipei, Taiwan